

Possible Constraints on the Density Dependence of the Nuclear Symmetry Energy from Quasiperiodic Oscillations in Soft Gamma Repeaters

Hajime Sotani¹ \star , Ken'ichiro Nakazato², Kei Iida³, and Kazuhiro Oyamatsu⁴

¹*Yukawa Institute for Theoretical Physics, Kyoto University, Kyoto 606-8502, Japan*

²*Faculty of Science & Technology, Tokyo University of Science, 2641 Yamazaki, Noda, Chiba 278-8510, Japan*

³*Department of Natural Science, Kochi University, 2-5-1 Akebono-cho, Kochi 780-8520, Japan*

⁴*Department of Human Informatics, Aichi Shukutoku University, 9 Katahira, Nagakute, Aichi 480-1197, Japan*

9 July 2018

ABSTRACT

We systematically examine the fundamental frequencies of shear torsional oscillations in neutron star crusts in a manner that is dependent on the parameter L characterizing the poorly known density dependence of the symmetry energy. The identification of the lowest quasiperiodic oscillation (QPO) among the observed QPOs from giant flares in soft-gamma repeaters as the $\ell = 2$ fundamental torsional oscillations enables us to constrain the parameter L as $L \geq 47.4$ MeV, which is the most conservative restriction on L obtained in the present work that assumes that the mass and radius of the flaring neutron stars range 1.4–1.8 M_{\odot} and 10–14 km. Next, we identify one by one a set of the low-lying frequencies observed in giant flares as the fundamental torsional oscillations. The values of L that can reproduce all the observed frequencies in terms of the torsional oscillations coupled with a part of dripped neutrons via entrainment effects are then constrained as $101.1 \text{ MeV} \leq L \leq 131.0 \text{ MeV}$. Alternatively, if only the second lowest frequency observed in SGR 1806–20 has a different origin, one obtains relatively low L values ranging $58.0 \text{ MeV} \leq L \leq 85.3 \text{ MeV}$, which seem more consistent with other empirical constraints despite large uncertainties.

Key words: relativity – stars: neutron – stars: oscillations – equation of state

1 INTRODUCTION

Neutron stars are believed to form as stellar remnants of core-collapse supernovae, which occur at the end of massive star evolution. The density of matter inside a neutron star can easily become higher than normal nuclear density, a situation hard to realize in the laboratory. Due to such high densities and resulting strong coupling nature, the equation of state (EOS) for neutron star matter remains to be fixed. Consequently, neutron stars act as a unique laboratory to constrain the properties of such dense matter. In fact, the discovery of a neutron star with $\sim 2M_{\odot}$ can rule out some of soft EOSs (Demorest et al. 2010). It is also suggested that information about neutron star interiors can be obtained via neutron star asteroseismology or via possible detection of the spectra of gravitational waves emitted from neutron stars (e.g., Andersson & Kokkotas (1996); Sotani, Tominaga & Maeda (2001); Sotani, Kohri & Harada (2004); Sotani et al. (2011)). Unlike gravitational waves, there are some observational evidences for neutron star oscillations, namely, quasiperiodic oscillations (QPOs) in giant flares from soft gamma repeaters (SGRs). Since SGRs are considered to be magnetars, which are neutron stars with strong surface magnetic fields of order $B \gtrsim 10^{14}$ – 10^{15} G, the observed QPOs could be strongly associated with neutron star oscillations. So far, three giant flares have been detected from SGR 0526–66, SGR 1900+14, and SGR 1806–20, respectively. The timing analysis of the X-ray afterglow of the giant flares shows that in two of them, specific oscillation frequencies arose in the range from tens of hertz up to a few kilohertz (Watts & Strohmayer 2006).

\star E-mail: sotani@yukawa.kyoto-u.ac.jp

After this discovery, many theoretical attempts to explain the observations have been made in terms of shear torsional oscillations in the crust of a neutron star and/or magnetic oscillations (e.g., Levin (2006, 2007); Lee (2007); Samuelsson & Andersson (2007); Sotani, Kokkotas & Stergioulas (2007, 2008a); Sotani, Colaiuda & Kokkotas (2008b); Sotani & Kokkotas (2009)). The important conclusion obtained from such attempts is that either the torsional oscillations or magnetic oscillations dominate the excited oscillations near the surface of a magnetized neutron star, depending on the magnetic field strength (Colaiuda & Kokkotas 2011, 2012; Gabler et al. 2011, 2012a) and magnetic configuration (Gabler et al. 2012b). Given the magnetic field strength inferred from the spindown observations (Kouveliotou et al. 1998; Hurley et al. 1999), we can reasonably consider the QPOs observed in giant flares as crustal torsional oscillations, especially in the case of low-lying modes (Passamonti & Lander 2013). This identification would allow one to probe the properties of matter in the crust, which are in turn related to the poorly known density dependence of the symmetry energy of nuclear matter (Steiner & Watts 2009; Sotani 2011; Gearheart et al. 2011; Sotani et al. 2012). Once the density dependence of the symmetry energy is fixed, furthermore, one can address the thickness of the region where nuclei of nonuniform pastalike structures (Lorenz et al. 1993; Oyamatsu 1993) occur in a neutron star (Oyamatsu & Iida 2007).

The deeper inside a neutron star, the more uncertainties in the EOS of neutron star matter. Between an ionic ocean near the star's surface and a fluid core, a crust occurs. In most of the crust, nuclei are believed to form a bcc Coulomb lattice in a roughly uniform electron sea. When the density becomes higher than about $4 \times 10^{11} \text{ g cm}^{-3}$, neutrons start to drip out of the nuclei, and some of them are expected to behave as a superfluid as long as the temperature is below the critical temperature. In fact, such superfluidity plays an important role in modeling pulsar glitches (Sauls 1989), while most of observed neutron stars are considered to be so cool that most of the dripped neutrons would behave as a superfluid in the absence of the lattice. According to the recent band calculations by Chamel (2012), however, a significant fraction of the dripped neutrons can be entrained non-dissipatively by protons in the nuclei via Bragg scattering off the lattice even at zero temperature. Meanwhile, neutron superfluidity due to the remaining dripped neutrons affects the crustal torsional oscillations, because such oscillations would be controlled by the enthalpy density of the constituents that comove with the protons (van Horn & Epstein 1990). There are earlier publications that examine the influence of neutron superfluidity on the torsional oscillations in the crust for a specific crust EOS in the Newtonian framework (Andersson, Glampedakis & Samuelsson 2009; Samuelsson & Andersson 2009; Passamonti & Andersson 2012), while we have recently performed systematic calculations in the relativistic framework, which were presented only briefly (Sotani et al. 2013a). In this paper, we thus present full details of such calculations, which give possible constraints on the parameter L characterizing the density dependence of the symmetry energy by comparing the fundamental frequencies of the shear torsional oscillations with the QPO frequencies observed in SGRs. We remark that Deibel, Steiner, & Brown (2013) performed a similar systematic analysis independently.

The paper is constructed as follows. In the next section, we describe the crust EOSs and equilibrium configurations that will be used for calculations of the crustal oscillation frequencies. In the third section, we give the perturbation equation that governs the shear torsional oscillations, as well as the boundary conditions, and then address how to take into account the effect of neutron superfluidity. In the fourth section, we show the numerical results for the oscillation frequencies and possible constraints on L . Finally, the paper closes with a conclusion. We adopt units of $c = G = 1$, where c and G denote the speed of light and the gravitational constant, respectively.

2 CRUST EQUILIBRIUM CONFIGURATION

We begin with the properties of matter in neutron star crusts, which are to some degree constrained by empirical data for nuclear masses and radii. Near the saturation point of symmetric nuclear matter at zero temperature, the bulk energy per nucleon can be written as a function of baryon number density n_b and neutron excess α (Lattimer 1981):

$$w = w_0 + \frac{K_0}{18n_0^2}(n_b - n_0)^2 + \left[S_0 + \frac{L}{3n_0}(n_b - n_0) \right] \alpha^2, \quad (1)$$

where w_0 , n_0 , and K_0 denote the saturation energy, saturation density, and incompressibility of symmetric nuclear matter. Meanwhile, S_0 and L are the parameters associated with the symmetry energy coefficients $S(n_b)$, i.e., $S_0 \equiv S(n_0)$ and $L \equiv 3n_0(dS/dn_b)$ at $n_b = n_0$. Among these five parameters, w_0 , n_0 , and S_0 are fairly well constrained by empirical masses and radii of stable nuclei, while the remaining two parameters L and K_0 are left uncertain (Oyamatsu & Iida 2003). To see how strongly the parameters are constrained, two of us (K.O and K.I) first constructed the model for the bulk energy $w(n_n, n_p)$ of nuclear matter as a function of neutron and proton number densities, $n_n = n_b(1 + \alpha)/2$ and $n_p = n_b(1 - \alpha)/2$, in such a way as to reproduce Eq. (1) in the limit of $n_b \rightarrow n_0$ and $\alpha \rightarrow 0$. Then, within a simplified version of the extended Thomas-Fermi theory in which the energy density functional for a nucleus of neutron number N and proton number Z ,

$$E = E_b + E_g + E_C + Nm_n + Zm_p, \quad (2)$$

with the bulk energy

Table 1. The EOS parameters adopted in the present analysis and the corresponding lower and upper densities of the pasta region. That is, n_1 denotes the baryon number density at which the nuclear shape changes from sphere to cylinder, while n_2 denotes that at which the nuclear matter becomes uniform.

y (MeV fm ³)	K_0 (MeV)	L (MeV)	n_1 (fm ⁻³)	n_2 (fm ⁻³)
-220	180	52.2	0.060	0.079
-220	230	73.4	0.064	0.073
-220	280	97.5	0.067	0.068
-220	360	146.1	0.066	0.066
-350	180	31.0	0.058	0.091
-350	230	42.6	0.063	0.086
-350	280	54.9	0.067	0.083
-350	360	76.4	0.072	0.076
-1800	180	5.7	0.058	0.134
-1800	230	7.6	0.058	0.127
-1800	360	12.8	0.058	0.118

$$E_b = \int d^3r (n_n(\mathbf{r}) + n_p(\mathbf{r})) w[n_n(\mathbf{r}), n_p(\mathbf{r})], \quad (3)$$

the gradient energy

$$E_g = F_0 \int d^3r |\nabla(n_n(\mathbf{r}) + n_p(\mathbf{r}))|^2, \quad (4)$$

the Coulomb energy

$$E_C = \frac{e^2}{2} \int d^3r \int d^3r' \frac{n_p(\mathbf{r})n_p(\mathbf{r}')}{|\mathbf{r} - \mathbf{r}'|}, \quad (5)$$

and the neutron (proton) rest mass m_n (m_p), was optimized with respect to the density distributions $n_n(\mathbf{r})$ and $n_p(\mathbf{r})$, which are for simplicity parametrized as

$$n_i(r) = \begin{cases} n_i^{\text{in}} \left[1 - \left(\frac{r}{R_i} \right)^{t_i} \right]^3, & r < R_i, \\ 0, & r \geq R_i, \end{cases} \quad (6)$$

where $i = n$ and p . Finally, for given $y \equiv -K_0 S_0 / (3n_0 L)$ and K_0 , the most relevant values of w_0 , n_0 , S_0 , and F_0 were obtained by fitting the charge number, mass excess, and charge radius, which can be calculated from the optimal density distribution, to the empirical values for stable nuclei. We remark that the parameter y corresponds to the slope of the saturation line in the vicinity of $\alpha = 0$ (Oyamatsu & Iida 2003).

In order to obtain the equilibrium nuclear shape and size as well as the crust EOS for various sets of y and K_0 at zero temperature, as in Oyamatsu (1993), Oyamatsu & Iida (2007) generalized Eqs. (2) and (6) to include dripped neutrons of uniform number density n_n^{out} , a neutralizing background of electrons of uniform number density n_e , and the lattice energy within a Wigner-Seitz approximation. As a result of optimization of the total energy density with respect to the parameters characterizing the nucleon distributions for given y and K_0 , the optimal energy density ρ and nucleon distributions were obtained as a function of n_b . As in Oyamatsu & Iida (2007); Sotani et al. (2012, 2013a), we here confine ourselves to the parameter range $0 < L < 160$ MeV, $180 \text{ MeV} \leq K_0 \leq 360$ MeV, and $y < -200 \text{ MeV fm}^3$, which equally well reproduce the mass and radius data for stable nuclei and effectively cover even extreme cases (Oyamatsu & Iida 2003). The EOS parameter sets adopted in the present analysis are tabulated in Table 1, where the baryon number densities n_1 at which the nuclear shape changes from sphere to cylinder and n_2 at which the nuclear matter becomes uniform are also listed. The interval between n_1 and n_2 corresponds to the pasta region, which decreases with L and vanishes at $L \sim 100$ MeV (Oyamatsu & Iida 2007). We remark that, in order to fill gaps in the values of L , which appear in Table I in Sotani et al. (2012), we add two more parameter sets, namely, $(y, K_0) = (-220 \text{ MeV fm}^3, 280 \text{ MeV})$ and $(-350 \text{ MeV fm}^3, 280 \text{ MeV})$, where the corresponding values of L are 97.5 and 54.9 MeV.

Let us now consider the equilibrium neutron star configurations. Since the magnetic energy is much smaller than the gravitational binding energy even for magnetars, we can neglect the deformation due to the magnetic pressure. Additionally, since the magnetars are relatively slowly rotating, we can also neglect the rotational effect. Hereafter, therefore, we consider spherically symmetric neutron stars, whose structure is described by the solutions of the well-known Tolman-Oppenheimer-

Volkoff (TOV) equations. In this case, the metric can be expressed in terms of the spherical polar coordinates r , θ , and ϕ as

$$ds^2 = -e^{2\Phi} dt^2 + e^{2\Lambda} dr^2 + r^2 d\theta^2 + r^2 \sin^2 \theta d\phi^2, \quad (7)$$

where Φ and Λ are functions of r . We remark that $\Lambda(r)$ is associated with the mass function

$$m(r) = \int_0^r dr' 4\pi r'^2 \rho(r') \quad (8)$$

as $e^{2\Lambda} = (1 - 2m(r)/r)^{-1}$.

To solve the TOV equations, one generally uses the zero-temperature EOS, i.e., the pressure p as a function of the energy density ρ . For matter in the crust, we use the same EOS models as described above. Unfortunately, the core EOS is still uncertain in the absence of clear understanding of the constituents and their interactions both in vacuum and in medium. Since we will focus on shear torsional oscillations that occur in the crust, we can effectively describe such uncertainties in the core EOS by solely setting the star's mass M and radius R as free parameters, without using specific models for the core EOS. In fact, for various sets of M and R , we systematically construct the equilibrium configuration of the crust by integrating the TOV equations with the crust EOS from the star's surface all the way down to the crust-core boundary as in Iida & Sato (1997); Sotani et al. (2012, 2013a). This is a contrast to the usual way of constructing a star by initially giving a value of the central mass density and then integrating the TOV equations with a specific model for the EOS from the star's center to surface. Hereafter, we will consider $1.4 \leq M/M_\odot \leq 1.8$ and $10 \text{ km} \leq R \leq 14 \text{ km}$ as typical values of M and R . Such choice of M and R can duly encapsulate uncertainties of the core EOS.

Generally, a restoring force for shear torsional oscillations is provided by shear stress, which comes from the elasticity of the oscillating body and is characterized by the shear modulus μ . In the case of torsional oscillations in the crust of a neutron star, the shear modulus is determined by the lattice energy of the Coulomb crystal that constitutes the crust. Since the crystal is generally considered to be of bcc type (an fcc lattice might occur in place of bcc in the crust as suggested by recent Thomas-Fermi calculations (Okamoto et al. 2012)), one can use the corresponding shear modulus, which is calculated for Ze point charges of number density n_i as

$$\mu = 0.1194 \times \frac{n_i (Ze)^2}{a}, \quad (9)$$

where $a = (3Z/4\pi n_e)^{1/3}$ is the radius of a Wigner-Seitz cell (Strohmayer et al. 1991). Note that this formula is derived in the limit of zero temperature from Monte Carlo calculations for the shear modulus averaged over all directions (Ogata & Ichimaru 1990). As shown in Sotani et al. (2012), the shear modulus depends strongly on the value of L , which comes mainly from the L dependence of the calculated Z (Oyamatsu & Iida 2007). It is natural that one should take into account the shear modulus in pasta phases, if present, but hereafter we simply assume $\mu = 0$ for the pasta phases, as in Gearheart et al. (2011); Sotani et al. (2012, 2013a). This is because the shear modulus in the pasta phases except a phase of spherical bubbles has at least one direction in which the system is invariant with respect to translation and hence is expected to be significantly smaller than that in a phase of spherical nuclei (Pethick & Potekhin 1998). Under this assumption, we have only to consider the shear torsional oscillations that are excited within a crustal region of spherical nuclei, i.e., for $n_b \leq n_1$. Anyway, the constraint on L that will be given below can be considered to be robust, because the pasta region is highly limited given the resulting constraint on L (Oyamatsu & Iida 2007).

3 TORSIONAL OSCILLATIONS

We now consider the shear torsional oscillations on the equilibrium configuration of the crust of a neutron star described above. In order to determine the frequencies, we adopt the relativistic Cowling approximation, i.e., we neglect the metric perturbations on Eq. (7) by setting $\delta g_{\mu\nu} = 0$. In fact, one can consider the shear torsional oscillations with satisfactory accuracy even with the relativistic Cowling approximation, because the shear torsional oscillations on a spherically symmetric star are incompressible and thus independent of the density variation during such oscillations. Additionally, due to the spherically symmetric nature of the background, we have only to consider the axisymmetric oscillations. Then, the only non-zero perturbed matter quantity is the ϕ component of the perturbed four-velocity, δu^ϕ , which can be written as

$$\delta u^\phi = e^{-\Phi} \partial_t \mathcal{Y}(t, r) \frac{1}{\sin \theta} \partial_\theta P_\ell(\cos \theta), \quad (10)$$

where ∂_t and ∂_θ denote the partial derivatives with respect to t and θ , respectively, while $P_\ell(\cos \theta)$ is the ℓ -th order Legendre polynomial. We remark that $\mathcal{Y}(t, r)$ characterizes the radial dependence of the angular displacement of a matter element. By assuming that the perturbation variable $\mathcal{Y}(t, r)$ has such a harmonic time dependence as $\mathcal{Y}(t, r) = e^{i\omega t} \mathcal{Y}(r)$, the perturbation equation that governs the shear torsional oscillations can be derived from the linearized equation of motion as (Schumaker & Thorne 1983)

$$\mathcal{Y}'' + \left[\left(\frac{4}{r} + \Phi' - \Lambda' \right) + \frac{\mu'}{\mu} \right] \mathcal{Y}' + \left[\frac{H}{\mu} \omega^2 e^{-2\Phi} - \frac{(\ell+2)(\ell-1)}{r^2} \right] e^{2\Lambda} \mathcal{Y} = 0, \quad (11)$$

where H is the enthalpy density defined as $H \equiv \rho + p$ with the energy density ρ and pressure p as described in Sec. 2, and the prime denotes the derivative with respect to r .

Once appropriate boundary conditions are imposed, the problem to solve reduces to an eigenvalue problem with respect to ω . Since there is no matter outside the star, we adopt the zero-torque condition at the star's surface. Meanwhile, since there is no traction force in the region with $\mu = 0$, we adopt the zero-traction condition at the position where spherical nuclei disappear in the deepest region of the crust. In practice, one can show that both conditions reduce to $\mathcal{Y}' = 0$ (Schumaker & Thorne 1983; Sotani, Kokkotas & Stergioulas 2007). Thus, in determining the frequencies of the shear torsional oscillations, we impose the condition of $\mathcal{Y}' = 0$ both at $n_b = 0$ and n_1 .

Now, we take into account the effect of neutron superfluidity on the shear torsional oscillations. In general, it is considered that neutrons confined in the nuclei start to drip therefrom when the mass density becomes more than $\sim 4 \times 10^{11}$ g cm $^{-3}$. Then, some of the dripped neutrons can behave as a superfluid. Although the behavior of the dripped neutrons is not fully understood, a significant fraction of the dripped neutrons may move non-dissipatively with protons in the nuclei as a result of Bragg scattering off the bcc lattice of the nuclei. In fact, the recent band calculations beyond the Wigner-Seitz approximation by Chamel (2012) show that the superfluid density, which is defined here as the density of neutrons unlocked to the motion of protons in the nuclei, depends sensitively on the baryon density above neutron drip and that a considerable portion of the dripped neutrons can be locked to the motion of protons in the nuclei. On the other hand, since the shear torsional oscillations are transverse, the remaining superfluid neutrons, whose low-lying excitations are longitudinal, do not contribute to such oscillations (Pethick, Chamel & Reddy 2010).

We build the effect of neutron superfluidity into the effective enthalpy density \tilde{H} , which can be determined by subtracting the superfluid mass density from the total enthalpy density H in Eq. (11) that fully contains the contributions of the superfluid neutrons as well as the nuclei and companions (Iida & Baym 2002). Since we assume that the temperature of neutron star matter is zero, the baryon chemical potential μ_b can be expressed as $\mu_b = H/n_b$. Thus, one can write down (Sotani et al. 2013a)

$$\tilde{H} = \left(1 - \frac{N_s}{A} \right) H, \quad (12)$$

where N_s denotes the number of neutrons in a Wigner-Seitz cell that do not comove with protons in the nucleus, while A is the total nucleon number in the Wigner-Seitz cell. Finally, substituting \tilde{H} for H in Eq. (11), one can determine the frequencies of the shear torsional oscillations, which include the effect of neutron superfluidity in a manner that depends on the value of N_s . Hereafter, we will assume that N_s comes entirely from the dripped neutron gas. Even so, it is still uncertain how much fraction of the dripped neutrons behave as a superfluid. Thus, as in Sotani et al. (2013a), we introduce a new parameter N_s/N_d , where N_d is the number of the dripped neutrons in the Wigner-Seitz cell. For $N_s/N_d = 0$, all the dripped neutrons behave as normal matter and contribute to the shear motion, while for $N_s/N_d = 1$, all the dripped neutrons behave as a superfluid. We remark that $N_d - N_s$ denotes the number of the dripped neutrons bound to the nucleus. Typically, the value of N_s/N_d depends on the density inside a neutron star (Chamel 2012), but the case of $N_s/N_d = 0$ in the whole crust is closer to the typical behavior than the case of $N_s/N_d = 1$.

In Fig. 1, we show the effective enthalpies for $N_s/N_d = 0$ by the solid lines and for $N_s/N_d = 1$ by the broken lines, where we adopt the EOSs with $y = -220$ MeV fm 3 and with $L = 52.2, 73.4, 97.5$ and 146.1 MeV. From this figure, one can see that the effective enthalpies for $N_s/N_d = 0$ are almost independent of the EOS parameters, while those for $N_s/N_d = 1$ depend strongly on the EOS parameters especially for $\rho \gtrsim 10^{13}$ g/cm 3 . This is because for larger L , the symmetry energy at subnuclear densities becomes smaller, leading to increase in the density of the dripped neutrons. Another important quantity that characterizes the shear torsional oscillations is the shear velocity v_s , which is defined as $v_s^2 \equiv \mu/\tilde{H}$. In Fig. 2, we depict the shear velocity with the same sets of the EOS parameters, where the solid lines are for $N_s/N_d = 0$ and the broken lines are for $N_s/N_d = 1$. From this figure, we find that, depending on N_s/N_d , the shear velocity can double that for $N_s/N_d = 0$. Both Figs. 1 and 2 suggest the necessity of introducing the effect of neutron superfluidity.

4 CONSTRAINTS ON THE EOS PARAMETERS

The shear torsional oscillations are often referred to as t -modes, which are labelled as $n_t\ell$, where ℓ is the angular index and n is the number of radial nodes in the eigenfunctions of the overtones for a specific ℓ . In order to see the dependence of the shear torsional oscillations on the EOS parameters, we first consider the case in which the effect of neutron superfluidity is ignored, i.e., $N_s/N_d = 0$. We calculate the fundamental frequencies of such oscillations for a typical neutron star model with $M = 1.4M_\odot$ and $R = 12$ km by using the 11 EOS parameter sets shown in Table 1. The calculated fundamental frequencies with $\ell = 2$ are shown in Fig. 3 as a function of L . From this figure, as in Sotani et al. (2012), one can see that the $\ell = 2$

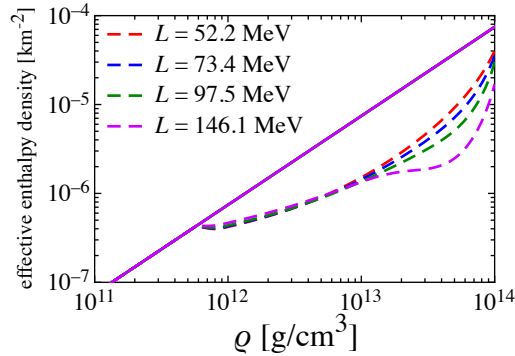


Figure 1. (Color online) Effective enthalpy density \tilde{H} calculated as a function of mass density ρ for $y = -220 \text{ MeV fm}^3$. The solid lines are the results for $N_s/N_d = 0$, while the broken lines are for $N_s/N_d = 1$. The four broken lines from top to bottom correspond to the cases of $L = 52.2, 73.4, 97.5$ and 146.1 MeV .

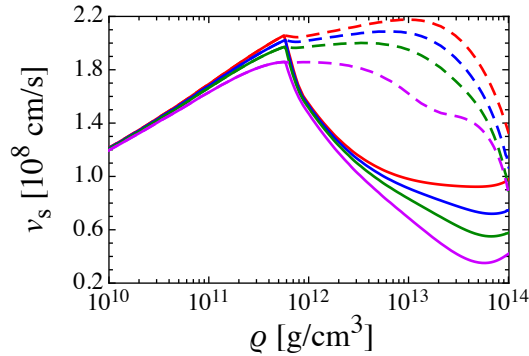


Figure 2. (Color online) Same as Fig. 1, but for the shear velocity v_s .

fundamental frequency of the shear torsional oscillations is almost independent of the incompressibility K_0 , once the stellar model is fixed at $M = 1.4M_\odot$ and $R = 12 \text{ km}$. So it is for different stellar models with $1.4M_\odot \leq M \leq 1.8M_\odot$ and $10 \text{ km} \leq R \leq 14 \text{ km}$. Thus, we can focus on the L dependence of the $\ell = 2$ fundamental frequencies of the shear torsional oscillations.

Since the number of the EOS parameter sets is limited to eleven, we want to see the L dependence in a continuous manner. To this end, we derive a fitting formula for ${}_0t_2$ by assuming the polynomial function form

$${}_0t_2 = c_2^{(0)} - c_2^{(1)}L + c_2^{(2)}L^2, \quad (13)$$

where $c_2^{(0)}$, $c_2^{(1)}$, and $c_2^{(2)}$ are the adjustable positive parameters that depend on M and R . In practice, we adopt the Levenberg-Marquardt algorithm to derive the coefficients $c_2^{(0)}$, $c_2^{(1)}$, and $c_2^{(2)}$. The obtained fitting formula is also shown in Fig. 3 with thick solid line. Additionally, for the stellar model with $M = 1.4M_\odot$ and $R = 12 \text{ km}$, we list the calculated $\ell = 2$ fundamental frequencies, ${}_0t_2^{(c)}$, the expected values from the fitting formula (13), ${}_0t_2^{(e)}$, and the relative errors defined as $({}_0t_2^{(c)} - {}_0t_2^{(e)})/{}_0t_2^{(c)}$ in Table 2. For other stellar models, the relative errors are similar to the case of $M = 1.4M_\odot$ and $R = 12 \text{ km}$. This means that the fitting formula is in good agreement with the calculated frequencies at least within the accuracy of $\sim 5\%$.

In Fig. 4, we illustrate the values of ${}_0t_2$ given by the fitting formula (13) for the stellar models with $10 \text{ km} \leq R \leq 14 \text{ km}$ and $1.4M_\odot \leq M \leq 1.8M_\odot$, together with the lowest QPO frequency observed from SGR 1806–20 shown in horizontal dot-dashed line. We remark that ${}_0t_2$ decreases with R and M . In Fig. 4, therefore, the upper (lower) boundary of the painted region corresponds to the $\ell = 2$ fundamental frequency for $M = 1.4M_\odot$ ($1.8M_\odot$) and $R = 10$ (14) km. Now, on the assumption that the QPOs observed in SGR giant flares come from the crustal torsional oscillations, ${}_0t_2$ should become equal to or even lower than the lowest frequency in the observed QPOs, because ${}_0t_2$ is theoretically the lowest frequency among many eigenfrequencies of the torsional oscillations. Then, from Fig. 4, we can constrain L as $L \geq 47.4 \text{ MeV}$ if the central objects of SGRs are neutron stars with $R \leq 14 \text{ km}$ and $M \leq 1.8M_\odot$. If the oscillating neutron star is a typical one with $R = 10 \text{ km}$ and $M = 1.4M_\odot$, we could make a severer constraint on L as $L \geq 76.2 \text{ MeV}$. It should be noticed that we omit the effect of the pasta phases on the shear modulus in this analysis. Given the resulting constraint on L , the pasta region is too limited to have significant consequence to ${}_0t_2$. In practice, even if we allow for the effect of the pasta phases, the frequency would increase because the shear modulus would effectively increase, i.e., the painted region in Fig. 4 would shift to right. Thus,

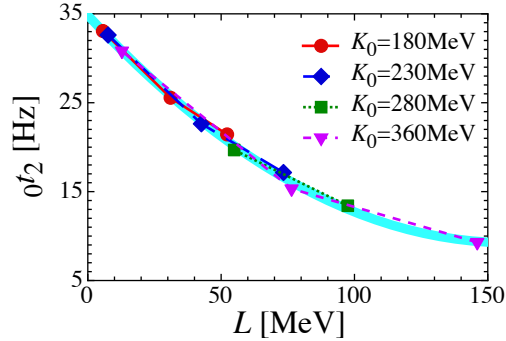


Figure 3. (Color online) The $\ell = 2$ fundamental frequencies of the shear torsional oscillations, ${}_0t_2$, which are plotted as a function of L for $M = 1.4M_\odot$ and $R = 12$ km. The thick solid line denotes the fitting formula (13).

Table 2. The calculated frequencies, ${}_0t_2^{(c)}$, for the stellar model of $M = 1.4M_\odot$ and $R = 12$ km in the absence of the effect of neutron superfluidity, and the expected values from Eq. (13), ${}_0t_2^{(e)}$. The relative errors, which are determined by $({}_0t_2^{(c)} - {}_0t_2^{(e)})/{}_0t_2^{(c)}$, are also tabulated.

y (MeV fm ³)	K_0 (MeV)	L (MeV)	${}_0t_2^{(c)}$ (Hz)	${}_0t_2^{(e)}$ (Hz)	relative error (%)
-220	180	52.2	21.44	20.73	3.31
-220	230	73.4	25.56	25.78	-0.86
-220	280	97.5	33.07	33.04	0.10
-220	360	146.1	17.15	16.60	3.17
-350	180	31.0	22.63	22.91	-1.24
-350	230	42.6	32.62	32.43	0.57
-350	280	54.9	13.41	13.02	2.96
-350	360	76.4	19.68	20.16	-2.43
-1800	180	5.7	9.29	9.40	-1.13
-1800	230	7.6	15.32	16.09	-5.00
-1800	360	12.8	30.82	30.86	-0.14

our constraint on L is still satisfied. Moreover, even if we take into account the effect of neutron superfluidity, the obtained constraint on L would hold, because the frequencies would increase due to the effect of neutron superfluidity (Sotani et al. 2013a).

Next, we consider the effect of neutron superfluidity on the torsional oscillations and try to constrain L by fitting the predicted fundamental frequencies of the shear torsional oscillations with different values of ℓ to the QPO frequencies observed in SGRs. To take into account the effect of neutron superfluidity, as mentioned before, one needs to know how much fraction of the dripped neutrons behave as a superfluid. In fact, earlier calculations of such a fraction are very limited, while the

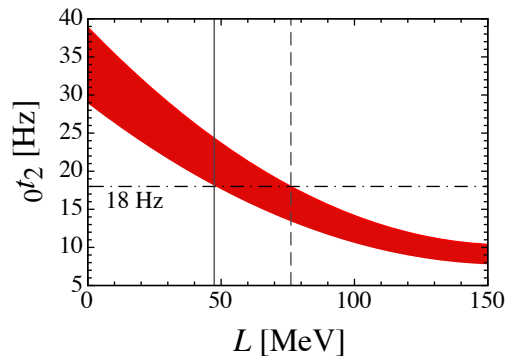


Figure 4. (Color online) Expected values of ${}_0t_2$ from fitting formula (13) for the stellar models with $10 \text{ km} \leq R \leq 14 \text{ km}$ and $1.4M_\odot \leq M \leq 1.8M_\odot$. The horizontal dot-dashed line denotes the lowest QPO frequency observed from SGR 1806-20 (Watts & Strohmayer 2006), while the vertical solid and broken lines correspond $L = 47.4$ MeV and $L = 76.2$ MeV.

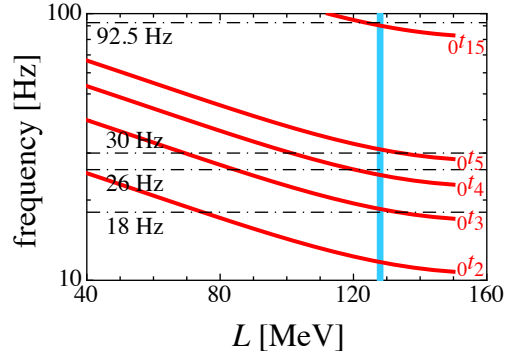


Figure 5. (Color online) Comparison of the calculated fundamental frequencies of the shear torsional oscillations (solid lines) with the QPO frequencies observed in SGR 1806–20 (dot-dashed lines), where we adopt the stellar model with $M = 1.4M_{\odot}$ and $R = 12$ km and the Chamel data for N_s/N_d . The vertical line denotes the value of L that is consistent with the observations.

behavior of unbound neutrons inside a nucleus remains to be fully understood. In this paper we adopt the result for N_s/N_d derived by Chamel (2012) as n_n^c/n_n^f , which is based on the band calculations. According to his data, the value of N_s/N_d depends on the baryon density and becomes around 10 – 30 % at $n_b \sim 0.01 - 0.4n_0$. We remark that this value of N_s/N_d does not allow for the possible dependence on L , which is still uncertain. Using such a value of N_s/N_d , we have calculated the fundamental frequencies of the shear torsional oscillations with different values of ℓ for the stellar models constructed with the EOS parameter sets as shown in Table 1. Then, we again find that, for each stellar model, the calculated frequencies show negligible dependence on K_0 but are sensitive to L as in the case of the calculations of $0t_2$ ignoring the superfluid effect.

To express the calculated $0t_{\ell}$ as a continuous function of L , we use the same form of fitting formula as Eq. (13):

$$0t_{\ell} = c_{\ell}^{(0)} - c_{\ell}^{(1)}L + c_{\ell}^{(2)}L^2, \quad (14)$$

where $c_{\ell}^{(0)}$, $c_{\ell}^{(1)}$, and $c_{\ell}^{(2)}$ are the adjustable positive parameters that depend on M and R for a specific index ℓ . We find that, just like the case of Eq. (13), Eq. (14) reproduces the calculated frequencies with sufficient accuracy to be used below for reasonable fitting to the observed QPO frequencies. Hereafter, we will thus refer to the expected frequencies from Eq. (14) as the calculated frequencies for simplicity. For comparison of the calculated frequencies with the observed QPO frequencies, we particularly focus on the observed QPO frequencies lower than 100 Hz, i.e., 18, 26, 30, and 92.5 Hz in SGR 1806–20 and 28, 54, and 84 Hz in SGR 1900+14 (Watts & Strohmayer 2006), because the higher observed frequencies would be easier to explain in terms not only of multipolar fundamental and overtone frequencies of shear torsional oscillations in the crust, but also of polar type oscillations. Additionally, the possibility to explain the higher QPO frequencies in terms of shear torsional oscillations in the hadron-quark mixed phase that may occur in the core of a neutron star is also suggested by Sotani, Maruyama & Tatsumi (2013b).

Due to the small interval between the observed frequencies 26 and 30 Hz in SGR 1806–20, theoretical explanations of the QPO frequencies observed in SGR 1806–20 are more difficult than those in SGR 1900+14 (Sotani, Kokkotas & Stergioulas 2007). Therefore, we first try to reproduce the QPOs observed in SGR 1806–20 by the crustal shear modes. To find a full correspondence of the shear torsional oscillations to the observed QPOs, one should identify the lowest frequencies in SGR 1806–20 (18 Hz) as the $\ell = 3$ fundamental frequency as in Sotani (2011); Sotani et al. (2013a). Then, one can manage to explain 26, 30, and 92.5 Hz in terms of the fundamental frequencies with $\ell = 4, 5$, and 15. In Fig. 5, we compare the predicted frequencies with the QPO frequencies observed in SGR 1806–20 for a typical neutron star model with $M = 1.4M_{\odot}$ and $R = 12$ km. The best value of L to reproduce the observed frequencies is $L = 128.0$ MeV, for which the calculated frequencies with the best value of L and their relative errors from the observed values are shown in Table 3. We note that the relative errors are of the order of such relative errors involved in using the fitting formula (14) as shown in Table 2. After performing a similar analysis for different stellar models, we find that the QPO frequencies observed in SGR 1806–20 can be explained in terms of the eigenfrequencies with the same multipole fundamental oscillations even for the different stellar models, while the corresponding relative errors are similar to those shown in Table 3. For each stellar model, the obtained best value of L is shown in Fig. 6. Assuming that the mass and radius of the oscillating neutron star are in the range $1.4 \leq M/M_{\odot} \leq 1.8$ and $10 \text{ km} \leq R \leq 14 \text{ km}$, one can constrain L as $101.1 \text{ MeV} \leq L \leq 160.0 \text{ MeV}$ from the observed QPO frequencies of SGR 1806–20.

On the other hand, the low-lying QPOs observed in SGR 1900+14 can be similarly explained in terms of the fundamental frequencies of the shear torsional oscillations with $\ell = 4, 8$, and 13. For the stellar model with $M = 1.4M_{\odot}$ and $R = 12$ km, we show, in Fig. 7, the calculated frequencies as a function of L and compare them with the QPO frequencies observed in SGR 1900+14. The best value of L to reproduce the observed frequencies in SGR 1900+14 is $L = 113.5$ MeV, for which the

Table 3. The QPO frequencies observed in SGR 1806–20 and the calculated frequencies with the best value of L to reproduce the observed values for the stellar model with $M = 1.4M_{\odot}$ and $R = 12$ km.

QPO frequency (Hz)	ℓ	${}_{0}t_{\ell}$ (Hz)	relative error (%)
18	3	18.50	−2.79
26	4	24.82	4.53
30	5	30.96	−3.19
92.5	15	90.18	2.51

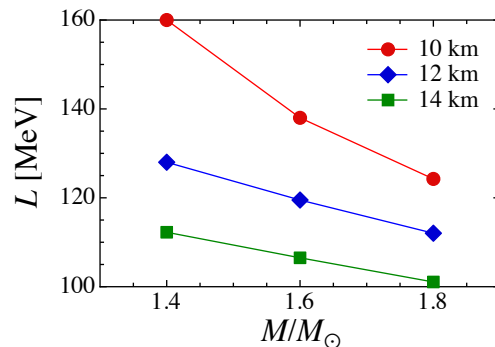


Figure 6. (Color online) Values of L at which the calculated fundamental frequencies of the shear torsional oscillations agree best with the QPO frequencies observed in SGR 1806–20. The circles, diamonds, and squares correspond to the stellar models with $R = 10$, 12, and 14 km, respectively.

calculated frequencies and relative errors are shown in Table 4. We can likewise obtain the best value of L to reproduce the observed QPO frequencies in SGR 1900+14 for each stellar model, which is plotted in Fig. 8. Assuming again that the mass and radius of the oscillating neutron star are in the range $1.4 \leq M/M_{\odot} \leq 1.8$ and $10 \text{ km} \leq R \leq 14 \text{ km}$, one can constrain L as $90.5 \text{ MeV} \leq L \leq 131.0 \text{ MeV}$ from the observed QPO frequencies of SGR 1900+14.

Note that both observations in SGR 1806–20 and in SGR 1900+14 should simultaneously be explained with a common value of L . We can thus obtain a more stringent constraint on L as $101.1 \text{ MeV} \leq L \leq 131.0 \text{ MeV}$, which is shown in Fig. 9. Some additional remarks are in order. First, such constraint on L in turn would constrain the masses and radii of the central objects in SGR 1806–20 and in SGR 1900+14 in such a way that the stellar models out of the painted region are ruled out. Such mass-radius constraints would be of particular use in the absence of empirical information about magnetar masses and radii. Second, within the nuclear model used here, as shown in Oyamatsu & Iida (2003), the symmetry energy at density n_0 , S_0 , can be approximately written as a function of L :

$$S_0 = 28 \text{ MeV} + 0.075L. \quad (15)$$

With this relationship, the constraint on L would translate into $35.6 \text{ MeV} \leq S_0 \leq 37.8 \text{ MeV}$. One might thus be able to make severer constraints on L and S_0 with the help of future possible measurements of magnetar masses and/or radii.

Meanwhile, as an alternative possibility, one can identify the three QPOs observed in SGR 1900+14 as the $\ell = 3$, 6, and 9 fundamental oscillations as in Steiner & Watts (2009). As shown in Fig. 10, this identification is reasonable and indeed seems to be in better agreement with the observations than the former one as the $\ell = 4$, 8, and 13 oscillations (see Table 5), although improvement in the degree of agreement, which is small compared with the intrinsic errors of the fitting formula (14) used here, may not have to be taken seriously. It is nonetheless interesting to note that the optimal values of L determined by

Table 4. Same as Table 3, but for the QPO frequencies observed in SGR 1900+14.

QPO frequency (Hz)	ℓ	${}_{0}t_{\ell}$ (Hz)	relative error (%)
28	4	27.26	2.63
54	8	53.76	4.50
84	13	86.18	−2.60

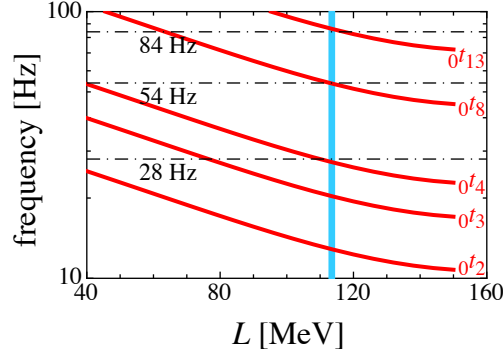


Figure 7. (Color online) Same as Fig. 5, but for comparison with the QPO frequencies observed in SGR 1900+14.

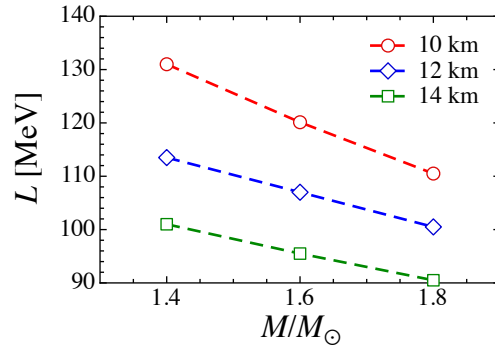


Figure 8. (Color online) Same as Fig. 6, but for the best agreement with the QPO frequencies observed in SGR 1900+14.

the identification as the $\ell = 3, 6,$ and 9 oscillations are in the range $58.0 \text{ MeV} \leq L \leq 89.5 \text{ MeV}$, as long as one assumes the stellar models with $1.4 \leq M/M_\odot \leq 1.8$ and $10 \text{ km} \leq R \leq 14 \text{ km}$. This is because such values of L are too small to become consistent with the optimal values of L based on the identification of the four QPOs in SGR 1806–20 as the $\ell = 3, 4, 5,$ and 15 oscillations.

To avoid such inconsistency, one could identify the 18, 30, and 92.5 Hz QPOs in SGR 1806–20 as the $\ell = 2, 3,$ and 10 oscillations as in Steiner & Watts (2009), although the 26 Hz QPO in SGR 1806–20 remains to be identified. In Fig. 11, we show how such an identification works for a typical neutron star model with $M = 1.4M_\odot$ and $R = 12 \text{ km}$; the corresponding relative errors are listed in Table 6. By identifying the low-lying QPOs except the 26 Hz QPO in SGR 1806–20 as the $\ell = 2, 3,$ and 10 shear torsional oscillations, one can obtain the optimal values of L as $54.0 \text{ MeV} \leq L \leq 85.3 \text{ MeV}$ for the stellar models with $1.4 \leq M/M_\odot \leq 1.8$ and $10 \text{ km} \leq R \leq 14 \text{ km}$, which, as in Fig. 12, ensures the presence of the allowed region of L that simultaneously explain both observations in SGR 1806–20 and in SGR 1900+14, i.e., $58.0 \text{ MeV} \leq L \leq 85.3 \text{ MeV}$.

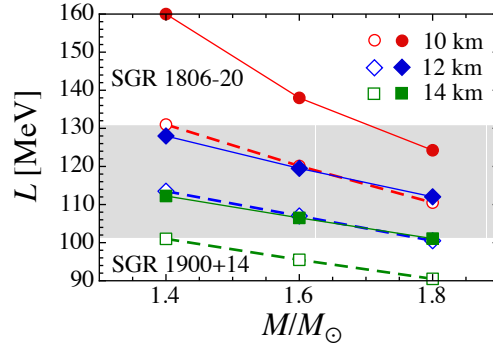


Figure 9. (Color online) The values of L (painted region) that are allowed simultaneously by both of the QPO observations in SGR 1806–20 and SGR 1900+14 on the assumption that the corresponding neutron stars have mass and radius in the range $1.4 \leq M/M_\odot \leq 1.8$ and $10 \text{ km} \leq R \leq 14 \text{ km}$.

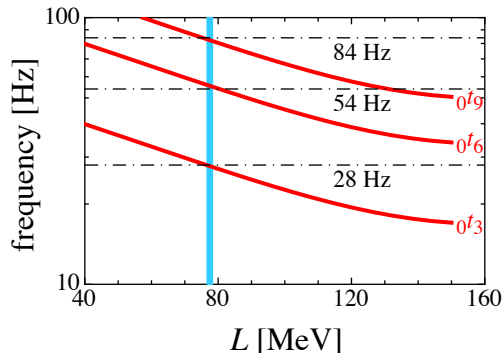


Figure 10. (Color online) Alternative possible correspondence between the calculated fundamental frequencies of the shear torsional oscillations and the QPO frequencies observed in SGR 1900+14. The vertical line denotes the value of L that is consistent with the observations.

Table 5. Same as Table 4, but for the alternative identification.

QPO frequency (Hz)	ℓ	${}_{0}t_{\ell}$ (Hz)	relative error (%)
28	3	27.74	0.93
54	6	55.48	-2.74
84	9	82.29	2.04

This region corresponds to $32.4 \text{ MeV} \leq S_0 \leq 34.4 \text{ MeV}$ via Eq. (15). We emphasize that the present identification is again in better agreement with the observed frequencies except 26 Hz than the former one as the $\ell = 3, 4, 5,$ and 15 oscillations. This may invoke the possibility that the physics underlying the 26 Hz QPO is missing. We remark that various experimental constraints on L seemingly favor smaller L , although they have yet to converge (see, e.g., Fig. 1 in Newton et al. (2012) and also Tsang et al. (2012)).

5 CONCLUSION

In this paper, we have investigated the fundamental frequencies of shear torsional oscillations in neutron star crusts, which contain superfluid neutrons, for nine sets of the star’s mass and radius as well as eleven models of the crust EOS, and considered possible relevance of the crustal shear modes to the QPOs observed from only a few SGRs in the afterglow of giant flares. We have succeeded in identifying the low-lying QPOs as the shear modes of different ℓ in two ways (one of which has an obvious caveat), leading to two separate allowed regions of the EOS parameter L characterizing the density dependence of the symmetry energy via reasonable fitting of the calculated mode frequencies to the observed QPO frequencies. The present

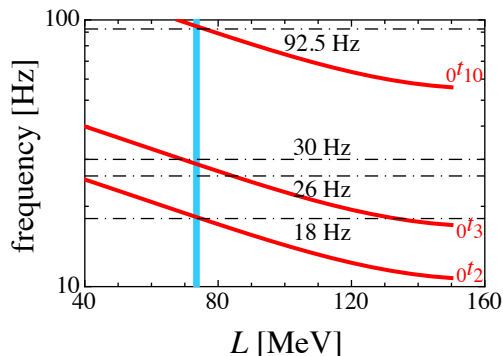
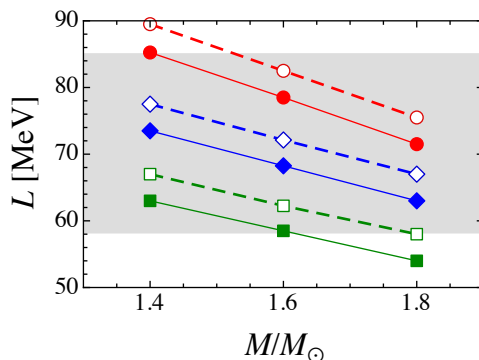


Figure 11. (Color online) Alternative possible correspondence between the calculated fundamental frequencies of the shear torsional oscillations and the QPO frequencies observed in SGR 1806–20 except 26 Hz. The vertical line denotes the value of L that is consistent with the observations.

Table 6. Same as Table 3, but for the alternative identification.

QPO frequency (Hz)	ℓ	$\omega_{t\ell}$ (Hz)	relative error (%)
18	2	18.23	-1.27
26	—	—	—
30	3	28.82	3.93
92.5	10	94.70	-2.38

**Figure 12.** (Color online) Same as Fig. 9, but for the alternative identification.

results are basically the same as those obtained in our earlier publications (Sotani et al. 2012, 2013a), but the present work is more systematic and quantitatively finer. We hope that future work in this direction, together with other empirical constraints on L , will eventually reduce the two allowed regions to one.

In order to obtain a better constraint on L asteroseismologically, however, many questions remain. Among various properties of crustal matter that control the shear torsional oscillations, the shear modulus and the superfluid density play an especially significant role. Estimates of the shear modulus in the Coulomb crystals of electron-screened, finite-size charges and in the liquid-crystalline pasta phases are thus desired, as well as of the local superfluid density throughout a Wigner-Seitz cell. For the bcc lattice of point charges, for example, the electron screening acts to reduce the shear modulus (Horowitz & Hughto 2008; Kobayakov & Pethick 2013), leading to decrease in the eigenfrequencies of the shear torsional oscillations typically by 5%. Meanwhile, shell and pairing effects on the nuclear charge, which are ignored in the present work, are expected to have some consequence to the shear modulus (Grill, Margueron, & Sandulescu 2011; Deibel, Steiner, & Brown 2013). Additionally, the crustal oscillations must be coupled with core magnetic oscillations if one considers a magnetized neutron star. For instance, Gabler et al. (2012a,b) showed that the frequencies of the crustal torsional oscillations can effectively increase, depending on the magnetic field strength and structure (dipole-like poloidal, mixed toroidal-poloidal with a dipole-like poloidal component and a toroidal field confined to the region of field lines closing inside the star, and for poloidal fields with an additional quadrupole-like component). On the other hand, it remains to be solved how to deal with the junction conditions at the interface between the crust and core regions, at least when one takes into account the effect of superfluidity inside both core and crust regions. Anyway we should also take into account the magnetic effect to obtain a better constraint on L , which will be addressed elsewhere.

This work was supported in part by Grants-in-Aid for Scientific Research on Innovative Areas through No. 23105711, No. 24105001, and No. 24105008 and for the global COE program “The Next Generation of Physics, Spun from Universality and Emergence” provided by MEXT, in part by Grants-in-Aid for Young Scientists (B) through No. 24740177 and for Research Activity Start-up through No. 23840038 provided by JSPS, and in part by the Yukawa International Program for Quark-hadron Sciences.

REFERENCES

- Andersson N., Kokkotas K. D., 1996, *Phys. Rev. Lett.*, 677, 4134
 Andersson N., Glampedakis K., Samuelsson L., 2009, *MNRAS*, 396, 894
 Chamel N., 2012, *Phys. Rev. C*, 85, 035801
 Colaiuda A., Kokkotas K. D., 2011, *MNRAS*, 414, 3014

- Colaiuda A., Kokkotas K. D., 2012, MNRAS, 423, 811
- Deibel, A. T., Steiner, A. W., Brown, E. F., 2013, preprint (arXiv:1303.3270)
- Demorest P. B., Pennucci T., Ransom S. M., Roberts M. S. E., Hessels J. W. T., 2010, Nature (London), 467, 1081
- Gabler M., Cerdá-Durán P., Font J. A., Müller E., Stergioulas N., 2011, MNRASL, 410, L37
- Gabler M., Cerdá-Durán P., Stergioulas N., Font J. A., Müller E., 2012a, MNRAS, 421, 2054
- Gabler M., Cerdá-Durán P., Font J. A., Muller E., Stergioulas N., 2012b, preprint (arXiv:1208.6443)
- Gearheart M., Newton W. G., Hooker J., Li B. A., 2011, MNRAS, 418, 2343
- Grill F., Margueron J., Sandulescu N., 2011, Phys. Rev. C, 84, 065801
- Horowitz C. J., Hughto J., preprint (arXiv:0812.2650)
- Hurley K. et al., 1999, Nature, 397, L41
- Iida K., Sato K., 1997, ApJ, 477, 294
- Iida K., Baym G., 2002, Phys. Rev. D, 65, 014022
- Kobyakov, D., Pethick, C. J., 2013, preprint (arXiv:1303.1315)
- Kouveliotou C. et al., 1998, Nature, 393, L235
- Lattimer J. M., 1981, Annu. Rev. Nucl. Part. Sci., 31, 337
- Lee U., 2007, MNRAS, 374, 1015
- Levin Y., 2006, MNRASL, 368, L35
- Levin Y., 2007, MNRAS, 377, 159
- Lorenz C. P., Ravenhall D. G., Pethick C. J., 1993, Phys. Rev. Lett., 70, 379
- Newton W. G., Gearheart M., Wen D. H., Li B. A., 2012, preprint (arXiv:1212.4539)
- Ogata S., Ichimaru S., 1990, Phys. Rev. A, 42, 4867
- Okamoto M., Maruyama T., Yabana K., Tatsumi T., 2012, Phys. Lett. B, 713, 284
- Oyamatsu K., 1993, Nucl. Phys. A, 561, 431
- Oyamatsu K., Iida K., 2003, Prog. Theor. Phys., 109, 631
- Oyamatsu K., Iida K., 2007, Phys. Rev. C, 75, 015801
- Passamonti A., Andersson N., 2012, MNRAS, 419, 638
- Passamonti A., Lander S. K., 2013, MNRAS, 429, 767
- Pethick C. J., Potekhin A. Y., 1998, Phys. Lett. B, 427, 7
- Pethick C. J., Chamel N., Reddy S., 2010, Prog. Theor. Phys. Suppl., 186, 9
- Ravenhall D. G., Pethick C. J., 1994, ApJ, 424, 846
- Samuelsson L., Andersson N., 2007, MNRAS, 374, 256
- Samuelsson L., Andersson N., 2009, Class. Quant. Gravity, 26, 155016
- Sauls J. A., in *Timing Neutron Stars*, edited by Ögelman H., van den Heuvel E.P.J. (Kluwer, Dordrecht, 1989), P. 457.
- Schumaker B. L., Thorne K. S., 1983, MNRAS, 203, 457
- Sotani H., Tominaga K., Maeda K. I., 2001, Phys. Rev. D, 65, 024010
- Sotani H., Kohri K., Harada T., 2004, Phys. Rev. D, 69, 084008
- Sotani H., Kokkotas K. D., Stergioulas N., 2007, MNRAS, 375, 261
- Sotani H., Kokkotas K. D., Stergioulas N., 2008a, MNRASL, 385, L5
- Sotani H., Colaiuda A., Kokkotas K. D., 2008b, MNRAS, 385, 2161
- Sotani H., Kokkotas K. D., 2009, MNRAS, 395, 1163
- Sotani H., 2011, MNRASL, 417, L70
- Sotani H., Yasutake N., Maruyama T., Tatsumi T., 2011, Phys. Rev. D, 83, 024014
- Sotani H., Nakazato K., Iida K., Oyamatsu K., 2012, Phys. Rev. Lett., 108, 201101
- Sotani H., Nakazato K., Iida K., Oyamatsu K., 2013a, MNRASL, 428, L21
- Sotani H., Maruyama T., Tatsumi T., 2013b, accepted for publication in Nucl. Phys. A
- Steiner A. W., Watts A. L., 2009, Phys. Rev. Lett., 103, 181101
- Strohmayer T., van Horn H. M., Ogata S., Iyetomi H., Ichimaru S., 1991, ApJ., 375, 679
- Tsang M. B. *et al.*, 2012, Phys. Rev. C, 86, 015803
- van Horn H. M., Epstein R. I., 1990, Bull. American Astron. Soc., 22, 748
- Watts A. L., Strohmayer T. E., 2006, Adv. Space Res., 40, 1446